Transient reconnection in the cusp during strongly negative IMF B_y

Y. Khotyaintsev,[1] S. Buchert,[1] K. Stasiewicz,[1] A. Vaivads,[1] S. Savin,[2] V. O. Papitashvili,[3] C. J. Farrugia,[4] B. Popielawska,[5] and Y.-K. Tung[6]

[1]   We investigate transient magnetic reconnection (flux transfer events, FTEs) in the cusp and its ionospheric signatures. We present in situ observations by the Polar spacecraft of multiple impulsive plasma injections and related magnetopause crossings in the outer stagnant cusp of the northern hemisphere. At this time the interplanetary magnetic field (IMF) was northward, dominated by strong B_y (-11 nT). Plasma injections are observed in the direction of the magnetic tension force due to the IMF B_y and resemble the "time of flight" energy-latitude dispersion. Associated magnetopause crossings exhibit large magnetic field rotation (>150 degrees) and strong depression of the field magnitude (down to several percent of the value in the magnetosheath). We use conjugate observations from the Greenland magnetometer network and Sondrestrom incoherent scatter radar together with the Polar UV imager to show that the transient reconnection causes a direct response of cusp auroral brightness and ionospheric convection in the direction consistent with the IMF B_y polarity. The observations, in space and on the ground, are consistent with a sequence of bulges launched by transient reconnection. We present a qualitative model of the bulge structure that is consistent with most of the Polar observations during the studied interval. Conjugate ground-based observations provide additional evidence for transient reconnection and are consistent with the ground signature of FTEs.   *INDEX TERMS:* 2724 Magnetospheric Physics: Magnetopause, cusp, and boundary layers; 2740 Magnetospheric Physics: Magnetospheric configuration and dynamics; 2736 Magnetospheric Physics: Magnetosphere/ionosphere interactions; 2437 Ionosphere: Ionospheric dynamics; *KEYWORDS:* cusp, magnetopause, reconnection

1.   Introduction

[2]   Magnetic reconnection is now widely believed to be the major process responsible for energy, momentum, and mass transfer from the solar wind to the magnetosphere. Open questions concern the spatial structure of the environment around magnetic reconnection sites, their location at the magnetopause in relation to the cusps, solar direction etc., and how this location is controlled, as well as the temporal evolution of reconnection including its ground signatures.

[3]   Spatially, the physics of reconnection involves a diffusion region where non-MHD processes govern the dynamics, surrounded by a larger field reversal (FR) region.

In the diffusion regions breaking of "frozen-in" conditions for ions and electrons, generation of parallel electric fields etc. can occur. Recent reports have found evidence for a diffusion region in in situ observations [*Scudder et al.*, 2002; *Mozer et al.*, 2002].

[4]   Earlier observations of magnetic signatures near the magnetopause, which are compatible with neither a tangential nor a rotational planar discontinuity, have indicated that field-line merging can be an intermittent process termed flux transfer events (FTEs) *Russell and Elphic* [1978]. Local dissipation in the diffusion region generates MHD waves and shocks propagating to the whole current layer and determining the properties of the field reversal (FR) region [*Petschek*, 1964]. For reconnection at the magnetopause (MP) the structure of the FR region is expected to be asymmetric with respect the MP plane due to plasma inflow from the magnetosheath (SH) only; generally, one observes a density decrease and an increase in magnetic field strength when going from the SH to the magnetosphere (MS). The structure of the FR region also becomes more complicated due to the transient character of reconnection. Models and simulations have described the formation of an asymmetric bulge in the outflow region [*Southwood et al.*, 1988; *Scholer*, 1989; *Semenov et al.*, 1992; *Kiendl et al.*, 1997]. The fast expansion and propagation of the bulge ($v \sim V_A$)

[1]Swedish Institute of Space Physics, Uppsala, Sweden.
[2]Space Research Institute (IKI), Moscow, Russia.
[3]Space Physics Research Laboratory, University of Michigan, Ann Arbor, Michigan, USA.
[4]Space Science Center and Department of Physics, University of New Hampshire, Durham, New Hampshire, USA.
[5]Space Research Centre, Polish Academy of Sciences, Warsaw, Poland.
[6]Space Sciences Laboratory, University of California, Berkeley, California, USA.

will cause the magnetic field compression on its front edge and a corresponding change in the total pressure [*La Belle-Hamer et al.*, 1995; *Semenov et al.*, 1997]. Observations of signatures of a FR region were reported from in situ measurements near the magnetopause [*Gosling et al.*, 1990; *Walthour et al.*, 1994; *Savin et al.*, 1998, 2001; *Fedorov et al.*, 2001; *Dubinin et al.*, 2002], from low-altitude spacecraft [e.g., *Lockwood and Moen*, 1996], and from sounding rockets [e.g., *Maynard et al.*, 2000].

[5] While spacecraft crossings of the magnetopause can be caused by reconnection bulges, they can also be caused by surface waves generated either due to solar wind pressure variations or Kelvin-Helmholtz (KH) instability. In reality, there may often be a mixture of several causes and the specific cause may be difficult to identify. For example this can be the case when the solar wind pressure variations themselves cause temporal variations in the reconnection process by alternately compressing and releasing the current sheet [*Sibeck and Newell*, 1995].

[6] It was known from early single spacecraft observations with Heos-2 and later Prognoz-7, 8, and 10 that generally the MP position and SH plasma flow structure are quite variable near the cusp, a region that is crucial for the entry of SH plasma into the MS [*Haerendel and Paschmann*, 1975; *Lundin et al.*, 1991]. The SH plasma in the vicinity of this indentation is highly disturbed and/or stagnant. The turbulent boundary layer (TBL) is a sub-region of the SH/cusp interface with nonlinear magnetic perturbations; it is located just outside and/or at the near cusp MP and has recently been found to be a permanent feature in this locale [*Haerendel*, 1978; *Savin et al.*, 1998, 2001].

[7] Most features seen in the topside ionosphere support the view that non-stationary merging is a globally relevant process. These include poleward moving transients seen in ground-based optical observations at 630 nm and 557.7 nm [e.g., *Sandholt et al.*, 1992], and flow bursts or channels in the plasma convection seen with HF radars [e.g., *Pinnock et al.*, 1993; *Neudegg et al.*, 2001] and also with incoherent scatter radar [e.g., *Lockwood et al.*, 1995]. Emissions in the UV associated with FTEs have been studied using the Polar satellite [*Milan et al.*, 2000; *Neudegg et al.*, 2001], revealing the characteristics of electron precipitation in the $1-5$ keV energy range. The ground-based signatures are typically consistent with a transient X line that is longitudinally extended over at least 3 hours of MLT [*Lockwood and Davis*, 1996] or longer [*Milan et al.*, 2000; *Pinnock et al.*, 2003].

[8] The presence of a significant IMF B_y results in asymmetric flows over the dayside magnetopause. The magnetic tension ($\mathbf{j} \times \mathbf{B}$) force acting on newly opened flux tubes leads to the asymmetric polar cap convection [*Jorgensen et al.*, 1972; *Gosling et al.*, 1990; *Freeman et al.*, 1990; *Siscoe et al.*, 2000], which is consistent with observations of westward or eastward flow bursts for strongly positive or negative B_y, respectively [*Lockwood and Davis*, 1996]. As the tension force acting on newly opened field lines decays, this east/west motion in the polar ionosphere is expected to develop into poleward motion. When the IMF B_y is negative (positive) the dawn (dusk) convection cell becomes dominant in the northern hemisphere; the effect is opposite in the southern hemisphere [*Papitashvili et al.*,

1994; *Weimer*, 1996; *Papitashvili and Rich*, 2002]. Such asymmetry produces a characteristic pattern in dayside magnetometer variations named as the Svalgaard-Mansurov effect [*Svalgaard*, 1968; *Mansurov*, 1969], and was commonly used as an indication of the IMF direction along the Parker spiral when no interplanetary measurements were available.

[9] The main goal of our study is to contribute to further understanding of transient reconnection at the magnetopause and its implications at ionospheric altitudes. This requires detailed studies of the reconnection sites, the reconnection bulges at the MP, and the phenomena observed by various instruments at the conjugate (to a satellite) ground sites. First, we study in detail the transient features in magnetic field and plasma flow observed in the outer cusp and determine the possible causes of these transient features. One possible cause is magnetic reconnection, which is likely to occur due to the antiparallel magnetic field configuration at the high-latitude MP close to the observation point. We reconstruct the structure of this region, and compare it to a structure of a reconnection bulge expected from simulations and previous observations. Subsequently, we study the effect of the transient features (FTEs) observed at the magnetopause on the ionospheric convection at the magnetic footprint, and discuss the role of these FTEs in the formation of global dayside convection.

[10] We base our study on an event observed on June 19, 1998, during which there is a conjugate observation by Polar located in the outer northern cusp and ground-based instruments in Greenland. This event is very germane for the purposes of our study because Polar, being close to apogee, moves very slowly and thus remains at the MP for a long time. Additionally, the solar wind is rather stable during the main period of interest, and the magnetic footprint of Polar remains close to one of the magnetometer stations. The paper is organized as follows. Section 2 shows observations made on board the spacecraft and at the ground observations, and other auxiliary data such as solar wind parameters and the spacecraft orbit. In section 3, we discuss possible interpretations of these observations. Section 4 contains a summary of our findings and conclusions.

2. Observations
2.1. Data Sources

[11] Spacecraft data used in this study are from the EFI [*Harvey et al.*, 1995], HYDRA [*Scudder et al.*, 1995], MFE [*Russell et al.*, 1995], TIDE [*Moore et al.*, 1995], and UVI [*Torr et al.*, 1995] instruments on board the Polar spacecraft. The ground-based data employed here are from the Greenland magnetometer network operated by Danish Meteorological Institute (DMI) and the Sondrestrom incoherent scatter radar operated by Stanford Research Institute (SRI) [*Kelly et al.*, 1995]. A list of the used magnetometer stations and their locations is presented in Table 1, the Sondrestrom ISR is collocated with the STF station. Solar wind data are from the MGF [*Kokubun et al.*, 1994] and CPI [*Frank et al.*, 1994] instruments on board the Geotail spacecraft.

2.2. Solar Wind Conditions

[12] Figure 1 presents magnetic field and plasma measurements from the Geotail spacecraft for $0900-1100$ UT

Table 1. Ground Stations Used[a]

IAGA Station ID	GEO		CGM	
	Lat	Long	Lat	Long
KUV	74.6	302.8	81.2	44.5
UMQ	70.7	307.9	76.9	43.9
GDH	69.3	306.5	75.8	40.4
ATU	67.9	306.4	74.6	39.0
STF[b]	67.0	309.1	73.2	41.7
SKT	65.4	307.1	72.0	38.0
GHB	64.2	308.3	70.6	38.5
FHB	62.0	310.3	68.0	39.7
MCG	72.6	321.7	76.3	62.1

[a]Columns give IAGA code of the station, the geographic latitude and longitude, and the corrected geomagnetic latitude and longitude of the station.

[b]Collocated with the Sondrestrom ISR.

on June 19, 1998; we examine mostly events occurring during the period of interest 1000–1030 UT. Geotail was located at (13.0, 25.6, −1.2) R_E GSE upstream of the bowshock. At 0925 UT the IMF began to turn northward from the southward B = (4, −5, −5 nT) conditions and there was also a corresponding increase in the solar wind density from 12 to 16 cm^{-3}. This lasted until 0940 UT, when the IMF increased in magnitude from 8 to 12 nT and became nearstationary B = (6, −11, 3 nT). The solar wind dynamic

pressure stayed approximately at the level of 4 nPa. Similar solar wind parameters were also observed (with relative time-shifts) on both the WIND and ACE spacecraft. According to the GSE X location of Geotail (13 R_E) the approximate propagation time for changes in the IMF between Geotail and the nose of the magnetosphere was about 1–2 minutes.

2.3. Polar Observations

[13] Figure 2 shows the Polar orbit for 0930–1100 UT on June 19, 1998. The spacecraft moves from (4.0, −4.9, 3.8) R_E GSE in the dawnside magnetosphere (MS) to (4.6, −4.4, 5.4) R_E GSE in the magnetosheath (SH). Figure 3 shows that multiple magnetopause (MP) crossings occurred after 1000 UT at a distance of 2.7 R_E from the model MP [*Shue et al.*, 1998]. MP crossings are seen as changes of B_y from positive values of 80 nT in the MS (which is close to the Tsyganenko's 2001 (T2001) model [*Tsyganenko*, 2000] values, dotted line) to negative values of −70 nT in the SH. On the basis of minimum variance analysis we conclude that GSE Y remains a good approximation for the direction of maximum variance for all MP crossings during the period of interest (1000–1030 UT). The direction of minimum variance (MP normal) changes between different crossings, but generally stays in the +X −Z sector in GSE. The mean MP location is crossed at 1041 UT, after which
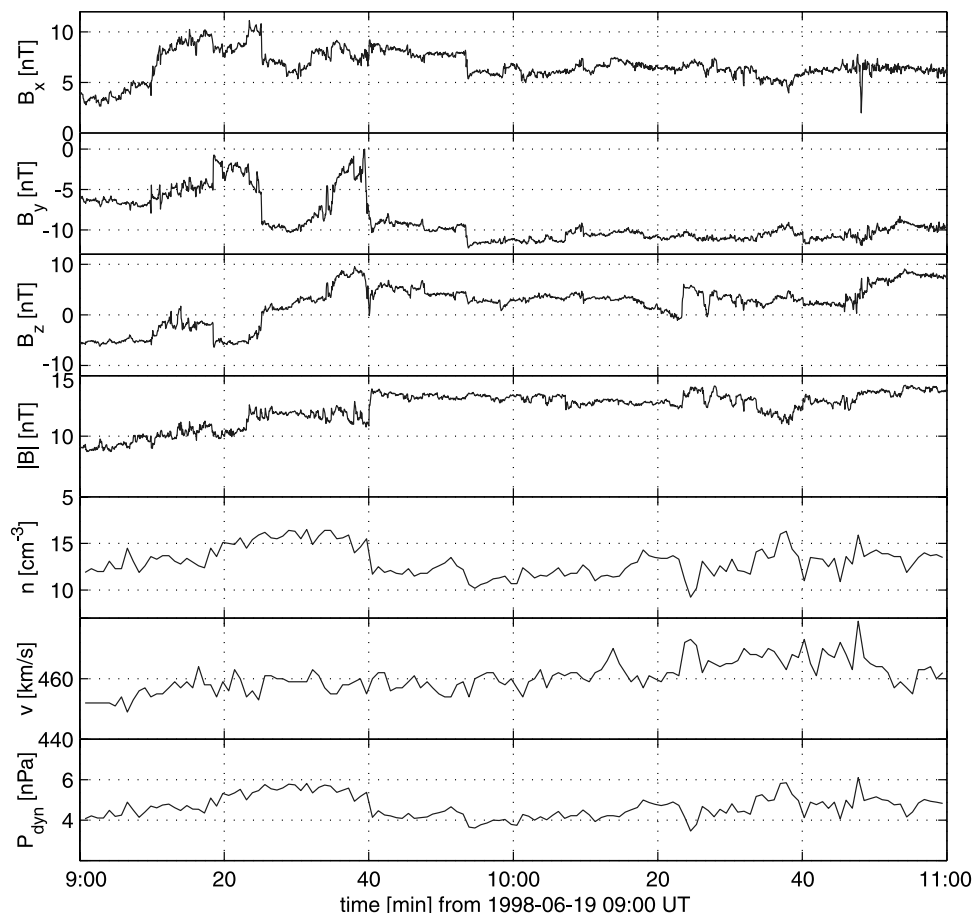

Figure 1. Solar wind data from Geotail for 0900–1100 UT on June 19, 1998. The panels show from top to bottom: the components in GSM coordinates and total magnitude of the IMF, and the solar wind density, velocity, and dynamic pressure.
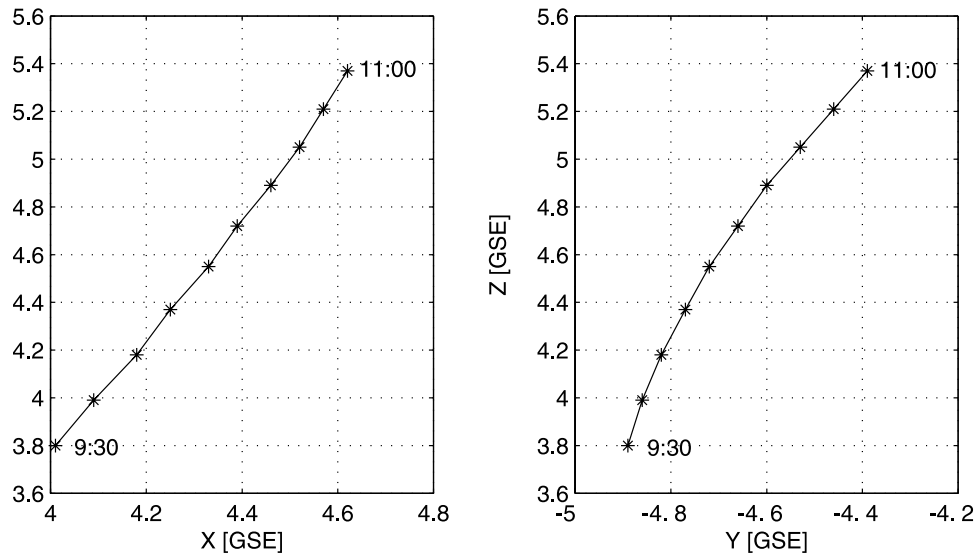
Figure 2. Polar orbit projections in the GSE XZ and YZ planes (in R_E) for 0930–1100 UT on June 19, 1998.

Polar was mainly in the SH, more specifically in the stagnation region near the northern cusp throat. The latter is identified by low SH flow velocities (see our discussion of Figure 4 below). We mainly concentrate on the period 1000–1030 UT, prior to the mean MP crossing, when Polar was for the most part on the magnetospheric side of the MP. The magnetic footprint of Polar traced with the T2001 model stays at almost the same location (in the CGM coordinates), moving slightly from 76.3° MLAT (61.4° MLONG) to 78.0° MLAT (56.6° MLONG).

[14] The plasma and magnetic field data from Polar for 1000–1045 UT are summarized in Figure 4 [see also *Dubinin et al.*, 2002; *Savin et al.*, 2002]. The five upper color panels show the antiparallel ($150 < \alpha < 180$, where α is the pitch angle) and parallel ($0 < \alpha < 30$) electron fluxes, and the antiparallel, perpendicular ($75 < \alpha < 105$) and parallel ion fluxes. Other panels display the electron anisotropy $T_{e\parallel}/T_{e\perp}$, ion perpendicular temperature, plasma density as measured by HYDRA (black) and derived from spacecraft potential (red), ion velocity components in GSE: V_x (black) and V_z (red), velocity V_y (black) and $\mathbf{E} \times \mathbf{B}$ velocity (red), total magnetic field magnitude (red) and B_y component (black). As the electric field measurement in the spin axis direction is not reliable, we assume $\mathbf{E} \cdot \mathbf{B} = 0$ to calculate this component from the spin plane components. This assumption is applicable during the period of interest since the magnetic field is directed away from the spin plane. Color stripes on the top and bottom of Figure 4 mark different regions described later in this section: black - inner magnetosphere, cyan - mantle, red - cusp, blue - magnetosheath boundary layer, green - magnetosheath. Parameters for the plasma and magnetic field of different regions crossed by Polar are summarized in Table 2.

[15] Polar was located in the inner magnetosphere from 0930 UT, with a short cusp encounter at 0940–0945 UT seen in Figure 3 as the B_y departure from the model value; the plasma was convecting sunward in this region. At 1004 UT, the density, electron and ion fluxes began increasing and the parallel plasma velocity V_{iy} became

negative (anti-earthward) marking the transition to the mantle. In addition the electron temperature distribution became more isotropic compared to the typical distribution for the closed field-lines; $T_{e\perp} > T_{e\parallel}$ before 1004 UT.

[16] The arrival of the first fast parallel (earthward) ions with energies 2–10 keV and onset of the parallel flow with velocity of 400 km/s at 1006 UT mark the transition to the cusp. There is a gradual increase in the ion temperature and density and a corresponding decrease in the magnetic field magnitude. The parallel flux consists of particles entering from the sheath, and the antiparallel flux from particles reflected from the ionosphere. In contrast to the electrons, only energetic ions will be fast enough to return back from
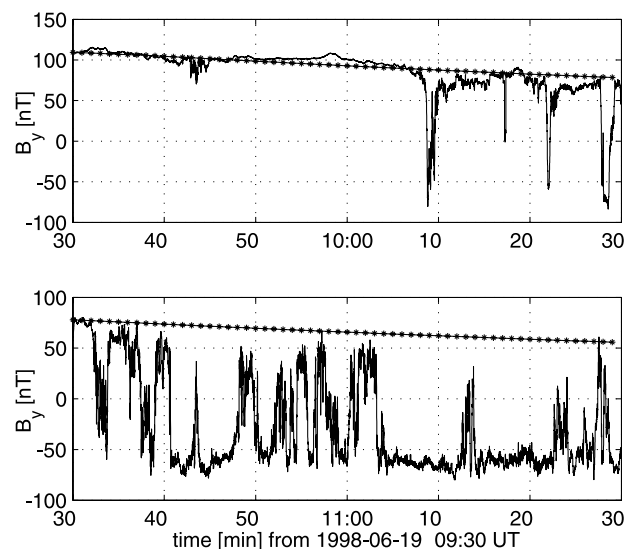

Figure 3. The B_y (GSE) component from Polar and Tsyganenko's 2001 model (dotted line) for 0930–1130 UT on June 19, 1998. The model of the magnetic field is calculated for the solar wind parameters observed by Geotail: B = (6;−11; 3) nT, p_{dyn} = 4 nPa.
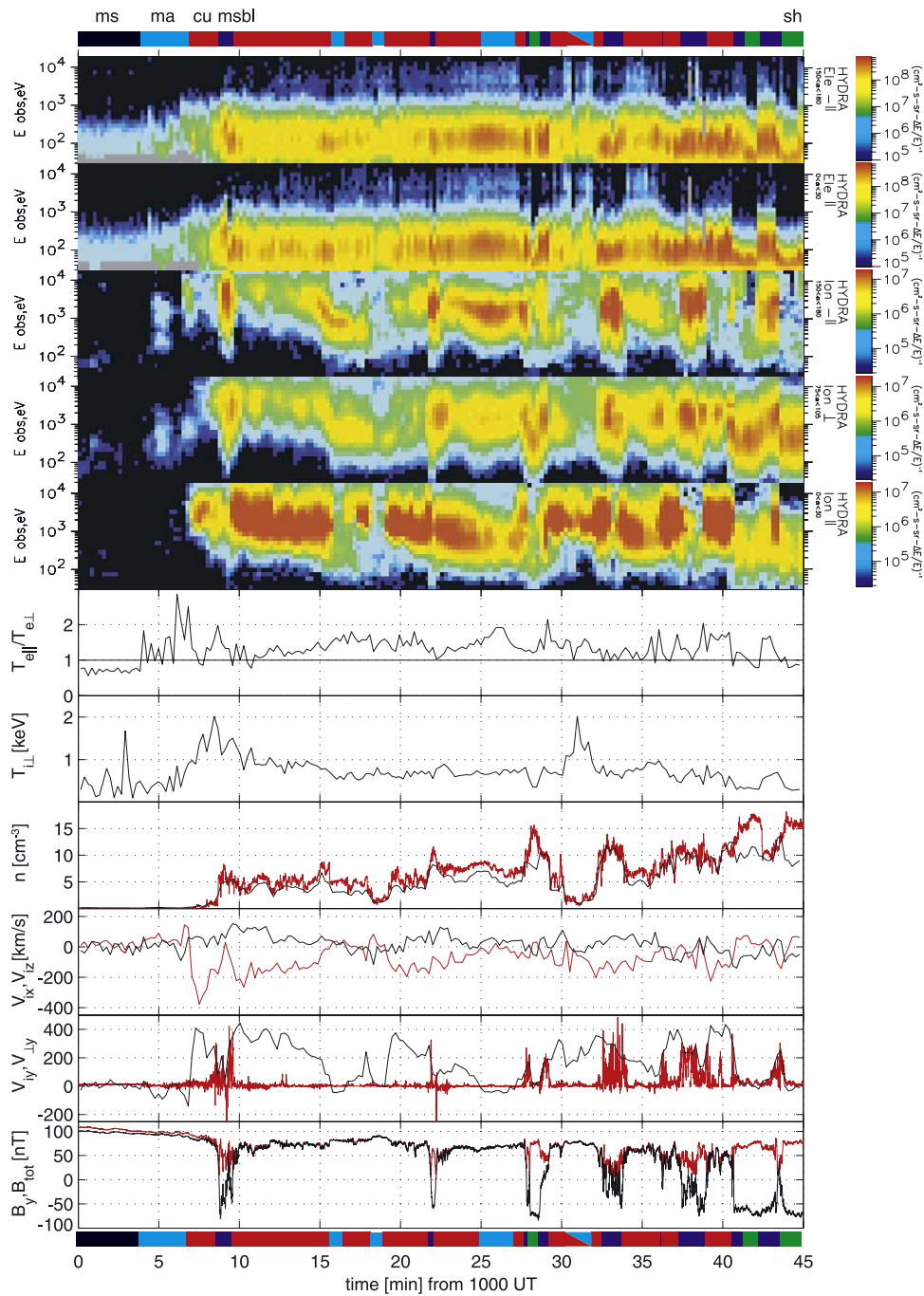
Figure 4. Polar spacecraft data for 1000–1045 UT on June 19, 1998.

the ionosphere to the same point in the cusp resulting in equal parallel and antiparallel fluxes at energies above 1 keV; the parallel flux is dominant at lower energies.

[17] The magnetopause crossing seen as the B_y reversal at 1008:40 UT marks the transition to the magnetosheath boundary layer (MSBL). The large depression in the magnetic field magnitude down to 10% of the MS value is associated with the field reversal. The transition is also well identified by an increase in the antiparallel flux (moving away from the MP), which is dominated by the heated/accelerated SH plasma reflected from the MP. The parallel and significantly colder flux consists of the inflowing SH

Table 2. Plasma and Magnetic Field Parameters for Different Regions[a]

Region	Inner MS	Mantle	Cusp	MSBL	SH
n, cm^{-3}	<0.1	3–6	4–6	~10	~10
B, nT	100	70–80	60–70	20–70	80
T_i, keV	0.1–0.6	0.5–0.8	0.6–1.0	0.3–0.8	0.2–0.3
T_e, 100eV	0.7–1.5	0.5–0.7	0.5–0.8	0.3–0.8	0.3–0.4
$T_{e\perp}/T_{e\|}$	>1	<1	<1	<1	1
V_{iy}, km/s	0	−50	200–400	200	−20

[a]Observed by Polar during the interval 1000–1045 UT, on June 19, 1998.

plasma. The spacecraft crosses the MP again and returns back to the cusp at about 1010 UT observing decaying parallel (earthward) ion flow.

[18] After 1015 UT the field-aligned flux of ions with energies below 1 keV is anti-earthward which is typical for the mantle-like plasma. A fresh parallel energetic ion injection happens at 1017 UT, which is interrupted by magnetic compression with drops in the ion flux and density down to 1 cm^{-3}. The MSBL is encountered at 1021:30 UT between the two MP crossings at 1021:30 and 1022:20 UT.

[19] As it returns to the MS, Polar observes the decaying parallel ion flow in the cusp gradually changing into the antiparallel mantle flow at 1025 UT and back to the cusp flow at 1027 UT. Another parallel energetic ion injection at 1027:30 UT is followed by the crossings of MP and MSBL. A short excursion into the magnetosheath is seen as a cessation of the parallel electron flux and a decrease of ion temperature. After returning into the cusp at 1029:20 UT, Polar observes another region of magnetic compression and low density between 1030 and 1032 UT. This is followed by two more cusp-MP-MSBL-MP-cusp passages with strong depressions of the magnetic field (sometimes <5 nT), with the final exit to the SH at 1041 UT. Plasma in the sheath is much colder and denser, $T_\perp > T_\parallel$ for both the ions and electrons. At 1043 UT there is a transition into the MSBL but this time from the SH side, followed by MP and cusp encounters and exit into the SH.

[20] Summarizing the observations during the period 1000–1045 UT, we note that there are three clear dispersive energetic ion injections in the earthward direction at 1006, 1017, and 1027 UT, followed by a very structured period after 1033 UT that shows multiple MP crossings and energetic ions without the well defined dispersion. Each event starts with an injection of ions of energy 2–10 keV in the direction parallel to the magnetic field, where corresponding parallel velocities increase to about 400 km/s. A slow decay lasting about 10 minutes follows. A detailed discussion of this structure follows in section 3.

2.4. Ionospheric Configuration

[21] The IMF turning from a southward (at 0940 UT) to a northward orientation and the appearance of a strong negative B_y after 0940 UT result in a change of the dayside ionospheric convection from the more symmetric pattern driven by negative B_z to the asymmetric one shifted in the direction of B_y and driven mainly by B_y. This convection response to the IMF rotation can be followed in the ground magnetometer data. Figure 5 shows the vertical (Z) component of the Greenland West Coast magnetometers; all stations are approximately at the same MLT $\approx$ UT-2h. The Z component increases when the chain moves toward the dayside indicating that the stations sense the cusp westward electrojet. The drastic change in the Z component, seen as a sign reversal from zero/positive to negative, first appears at lower latitudes (about 68° MLAT) right after the stabilization of IMF at 0945 UT, and then propagates further north up to $\sim$77° MLAT at 1015 UT. The stations above 72° MLAT experience an additional increase in the Z component preceding the change of sign. The most poleward KUV station shows the increase in the Z component but does not see the sign change, and remains at $\sim$500 nT for about 1 hour. All of this is consistent with the fast poleward
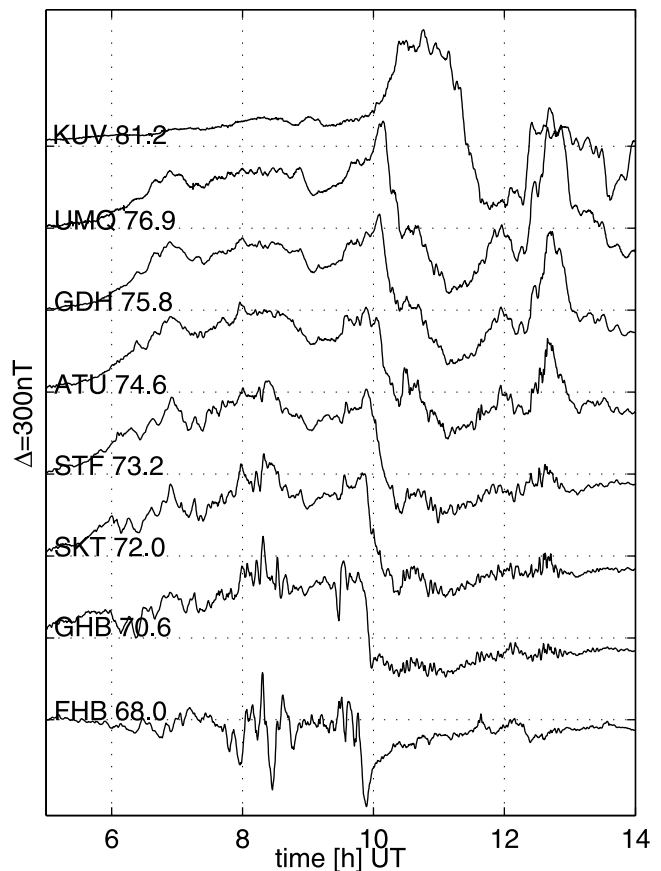
Figure 5. The Z component from the Greenland West Coast magnetometer chain for 0500–1400 UT on June 19, 1998. The distance between baselines is 300 nT.

motion of the cusp westward electrojet from about 68° to 78° MLAT as a response to the IMF change. Longitudinally, the enhanced electrojet (flow channel) extends from 07 MLT to 11 MLT, as seen simultaneously by the West Coast, Ice Cap, and East Coast magnetometers (not shown).

[22] The incoherent scatter radar data also show features related to the poleward moving channel of eastward flow as it is expected for a negative B_y in this event. Figure 6 presents the Sondrestrom ISR observations, which is collocated with the STF magnetometer station. The F-region ion temperature is locally enhanced indicating the enhanced plasma convection; consistent with this the strong eastward flow (2000 m/s), which appears after 0950 UT (earlier data are not available) at lower latitudes (about 70–71° MLAT), propagates poleward, reaching latitudes above 78° MLAT at 1015 UT.

[23] To see the global picture of the situation on the ground we present a sequence of the auroral images obtained by the Polar UV Imager between 1006 UT and 1021 UT on Figure 7. The individual images are separated in time by approximately 3 minutes. The day-glow is removed from these images and the dayside aurora can be seen more clearly. The magnetic footprint of Polar is marked by a cross and can be seen in the middle of Greenland (321° LONG, 72° LAT; 77° MLAT, 60° MLONG). We are mainly interested in the part of the dayside auroral oval over Greenland. The aurora is clearly seen near the Polar
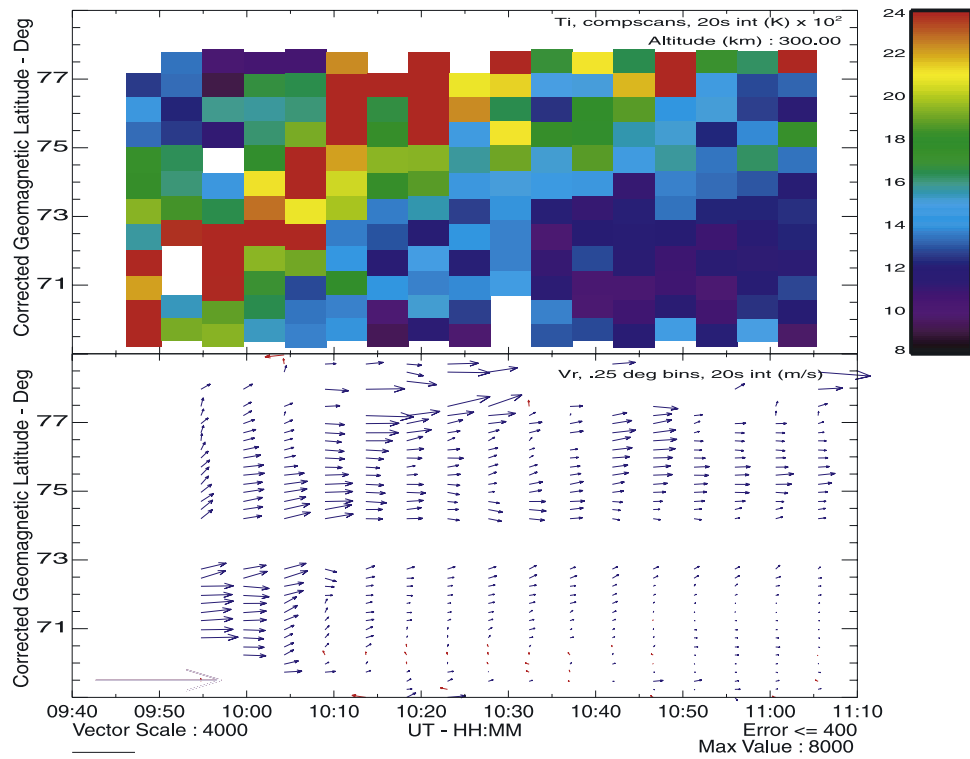
Figure 6. Data from Sondrestrom ISR for 0940–1110 UT on June 19, 1998. F-layer (300 km) T_i (upper panel), convection velocity (lower panel).

footprint approximately in the same location as the enhanced convection detected in the radar and magnetometer data. Variations in aurora intensity are discussed in the next section.

2.5. Satellite-Ground Correlations

[24] In this section, we study in detail the correlation between the plasma injection events observed by Polar and the changes in ionospheric convection. Figure 8 presents the horizontal magnetic disturbance vectors combined from the H (local magnetic north) and E (local magnetic east) components for the Greenland West Coast stations and for the Ice Cap station MCG, which is the closest to the magnetic footprint of Polar. As discussed in the previous section, the main feature observed here is the global convection change in response to the IMF turning at 0945 UT, which is seen in Figure 8 as a poleward propagating large negative disturbance of the H component corresponding to the cusp westward electrojet (eastward convection channel). This large scale feature contains a smaller scale substructure which can be related to the plasma injection events detected by Polar at the MP. These small scale variations (marked by red bars in Figure 8) are occurring quasi-periodically with period of ∼10 min as an eastward turning and increase of magnitude of the horizontal component.

[25] The signature of the first plasma injection event (1006 UT) is observed when the large scale convection variation reaches the magnetic footprint of Polar. The most drastic changes are seen in the H and Z components measured at the MCG station (Z not shown), which is approximately in the magnetic footprint of Polar. The H component reaches the minimum of −600 nT and the Z component changes sign to negative at 1006 UT, indicating

Figure 7. Sequence of images from Polar UVI for 1006–1021 UT on June 19, 1998. The magnetic footprint of Polar is marked by the blue cross.

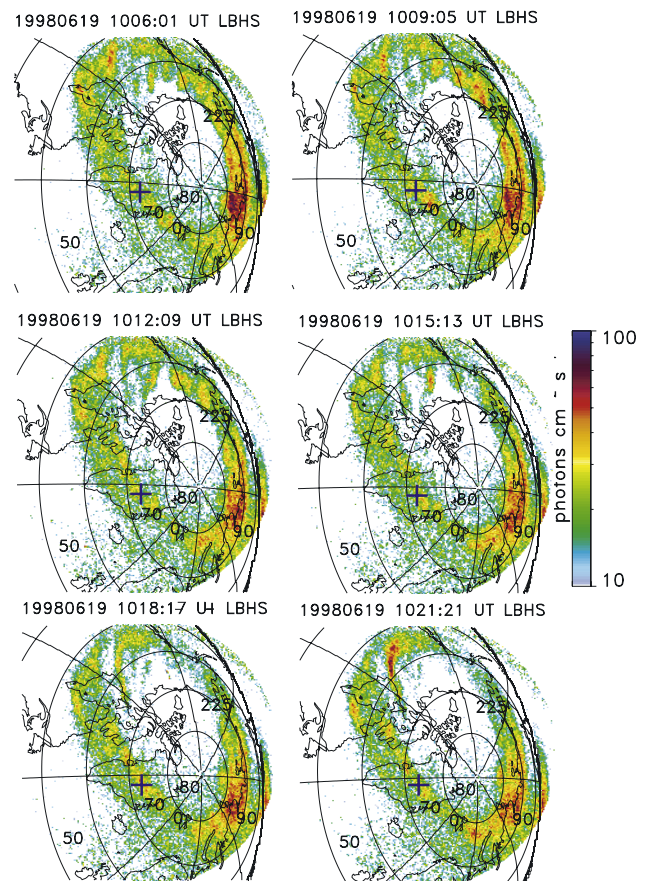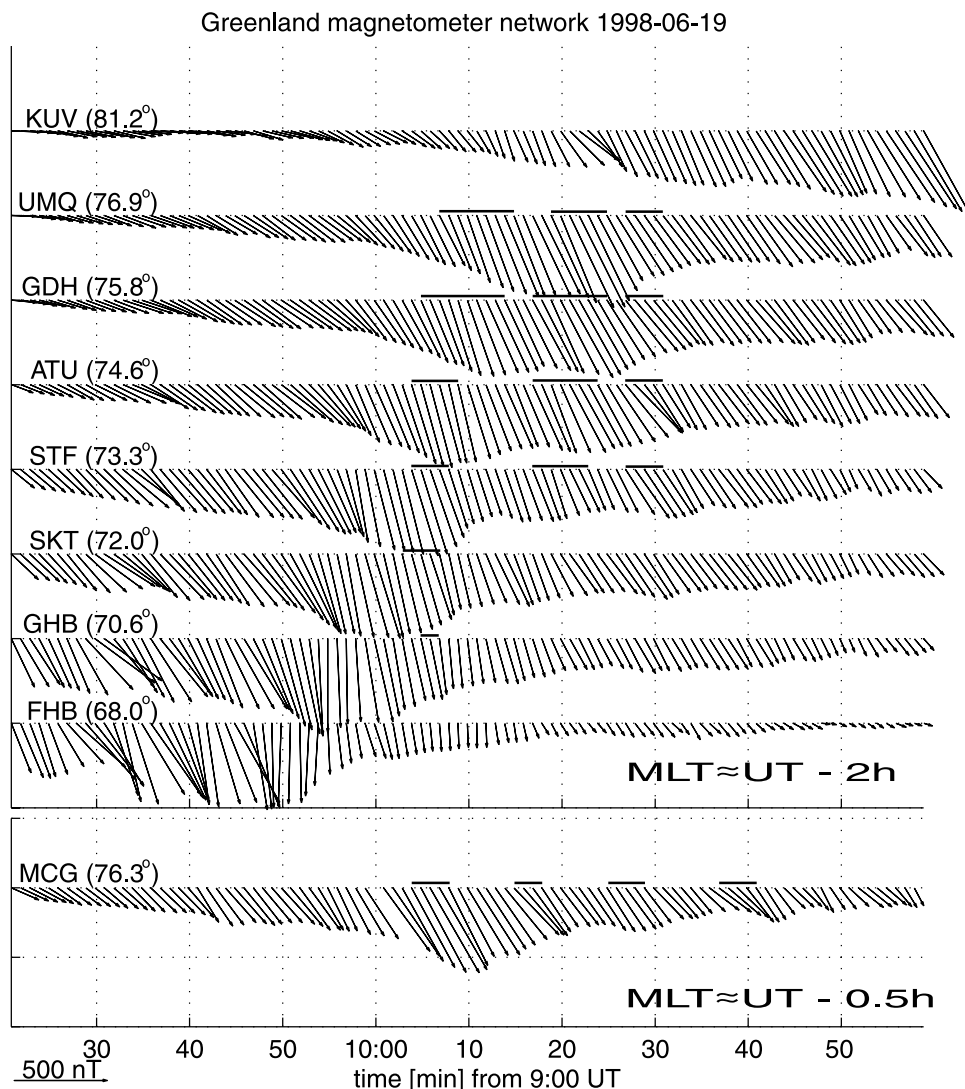**Figure 8.** Horizontal components from the Greenland West Coast magnetometer chain for 0900–1100 UT on June 19, 1998. The X and Y axes of the plot correspond to the magnetic eastward and northward directions, respectively. Black bars mark small scale variations (changes in direction and amplitude) seen in connection with plasma injection events observed by Polar.

that the convection channel passed the MCG station and then stayed poleward of it. The strongest H variation occurs almost simultaneously with the detection of the first fast ions by Polar. The small scale ionospheric signature is seen in Figure 8 as an increase in the magnitude and eastward turning of the total horizontal magnetic vector that corresponds to the intensification and poleward turning of the convection flow. The maximum variation of the H and E components is observed by SKT (72.0° MLAT) and STF (73.2° MLAT) at 1004 UT. In two minutes this variation reaches MCG which is the closest station to the footprint of Polar (76.3° MLAT, 61.4 MLONG at 1000 UT). The increase in the convection at 74–75° MLAT is also seen in the Sonderstrom ISR data (Figure 6) between 1000 and 1010 UT. The maximum convection velocity is about 2 km/s. A UV intensity observed by UVI at 1009 UT (Figure 7) in the region of strong convection is enhanced in comparison with the nearby images. The aurora extends by ~3 degrees

in latitude, and by ~2 hours in MLT. The brightest UV spot is seen at the 1009 UT image east from the footprint of Polar.

[26] The signature of the plasma injection event at 1017 UT is very similar to the first event (1006 UT), but it occurred poleward of this by approximately 2 degrees. The strongest magnetometer signature is observed by the GDH and UMQ stations (75.8–76.9° MLAT) at 1018 UT and the corresponding convection increase is seen on latitudes above 76° in the Sonderstrom ISR data after 1010 UT (Figure 6). The brightest aurora connecting UMQ and the footprint of Polar is seen in the UV image at 1018 UT (Figure 7). The aurora extends by more than 3 hours in MLT this time. The image at 1021 UT shows a similar location of the aurora, but overall intensity is lower with the exception of two bright spots.

[27] Unlike the first plasma injection events (1006 and 1017 UT) which seem to be associated with the peak of

global convection variation, the event at 1027 UT occurs during the relaxation phase as seen from the magnetometer data in Figure 8; it does not have any significant signatures in the radar data. This may be caused by the fact that the footprint of Polar and the convection channel itself moved out of the ISR's field of view. The signature in the UVI data is similar to the previous events, but has a lower intensity.

3. Discussion

3.1. Satellite Observations

[28] Polar observations show multiple events of energetic ion injections and associated crossings of the MP. Antiparallel magnetic merging, which is likely to occur on the dawn flank in the northern hemisphere under conditions of northward IMF with a strong negative B_y, is a possible candidate for explaining these observations. There are several strong arguments in favor of reconnection producing the observed structure of the MP: (1) magnetic field configuration is close to antiparallel in the MS and SH (Y and −Y in GSE, respectively), (2) accelerated plasma flows are very coherent and aligned along the GSE Y direction (in accordance with the IMF B_y tension force), (3) these plasma flows are observed on open magnetospheric field lines, (4) energy dispersion of energetic ions is observed.

[29] As for the causes of magnetopause indentation, solar wind pressure and KH waves must be considered in addition to reconnection. Solar wind pressure variations cannot be excluded, because some pressure variations are seen in Geotail data, and additional variations can be created in the foreshock region [Sibeck et al., 1989, 2003; Fairfield et al., 1990]. The KH instability usually has maximum growth at wavelengths that are of the order of ten times the MP thickness. For our case this would give wavelength of the order a few R_E or time scales of order one minute. This is not far from the typical time scales of the MP indentations seen in our data. However, solar wind pressure pulses and KH or TBL waves cannot explain the flows in GSE Y-direction or the observed ion dispersion. It does not seem that these mechanisms are able to explain significant transport of plasma (especially electrons) into the MS [Smets et al., 2002]. Thus once more we cannot exclude that indentation of the MP can be caused by one of these mechanisms, though we still would need reconnection to explain other observed features.

[30] We would like to compare our observations with two possible models: (1) plasma acceleration and MP motion are caused by transient reconnection (FTE), (2) plasma acceleration is caused by steady reconnection, while MP motion is caused by some other mechanism. First we test the transient reconnection scenario, where magnetic field and flow changes observed by Polar are caused by bulges that are launched intermittently from the reconnection site and later hit the spacecraft [Fedorov et al., 2001; Dubinin et al., 2002]. A schematic of a "switch-on" reconnection bulge inferred from the observations is presented in Figure 9. One must note that in reality the bulge is much more elongated along the MP than on this sketch. It is possible to identify several distinct regions in the vicinity of the bulge. The SH (region 1′) and MS (region 1) are the regions with oppositely oriented magnetic fields which begin to reconnect.
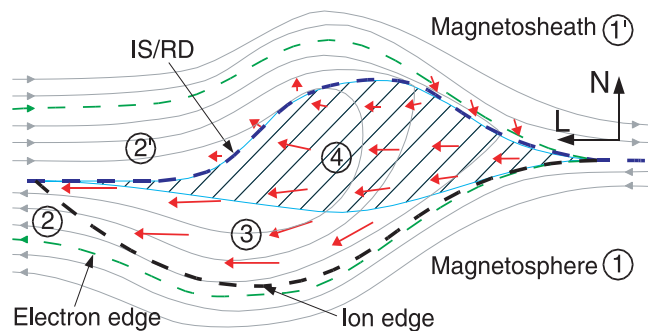
Figure 9. A schematic of the magnetopause region during transient reconnection. Plasma flow direction is marked with arrows.

The magnetosheath boundary layer (MSBL, region 2′) is located upstream of the bulge on the SH field-lines which are newly reconnected. It contains two main plasma populations: inflowing (parallel to **B**) cold SH plasma and counterstreaming accelerated and heated (at the MP) plasma. The boundary (MP) separating the regions 2′ and 4 is either a rotational discontinuity or an intermediate shock, containing the largest magnetic field, density and temperature jumps from SH to MS values. The magnetic field experiences a significant drop in magnitude at this discontinuity. The rest of the rotation in **B** happens in region 4. The SH plasma enters the MS through the discontinuity and region 4, where it is accelerated by the $\mathbf{j} \times \mathbf{B}$ force forming a plasma jet concentrated at the magnetospheric side of the MP. The plasma flow in region 4 is mainly perpendicular to **B**, driving the convectional electric field. Noticeable plasma heating also occurs at the discontinuity.

[31] The dense and heated SH plasma streaming parallel to the magnetic field from region 4 forms the cusp (region 3). The particle distributions resemble the "time of flight" dependency, when particles with large parallel velocities are observed at larger distances from the source of acceleration. The boundary at which the first sheath ions (electrons) are observed is the ion (electron) edge. Close to the ion edge the density of the sheath ions is low, but their high parallel velocity leads to a large bulk velocity. The density slowly increases with distance from the ion edge while magnetic field magnitude decreases so that the total pressure is conserved throughout the region. A magnetic barrier exists from the magnetospheric side of bulge, controlling the expansion of the bulge plasma.

[32] Figure 10 shows the plasma injection event observed by Polar during the interval 1005–1016 UT (see also Figure 4), which we believe is a crossing of a reconnection bulge. The numbers on the top mark different regions according to Figure 9. Combination of the motion across the MP and parallel motion of the bulge would make a spacecraft located close to MP cross the bulge, then exit into the MSBL, and then return back into the MS. The observations can then be explained in the following manner. First Polar was in region 1 and observed the magnetic compression/barrier and the electron and ion edges at 1006:00 and 1006:30 UT, respectively. Region 3 shows ions streaming parallel to **B** with decaying energy and increasing density. The magnetic field slowly decreases, so that the total
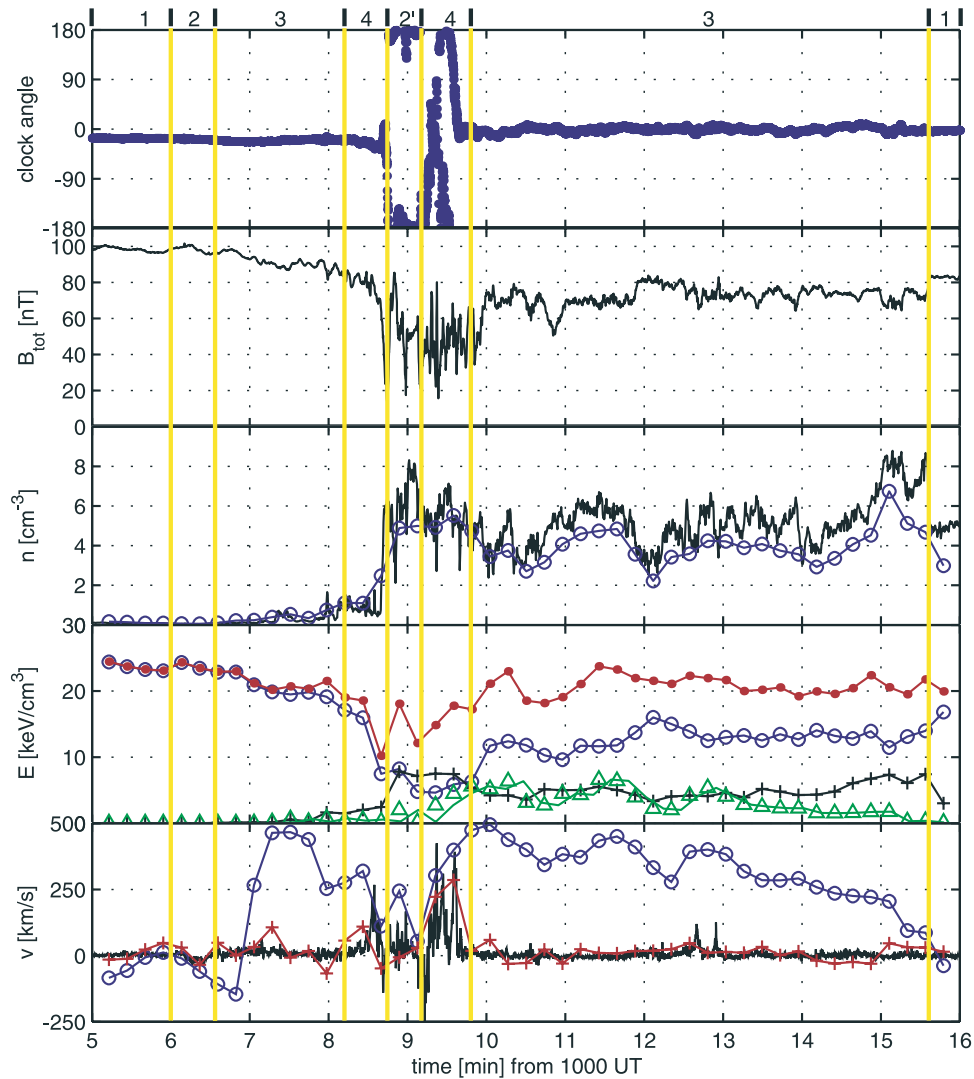
Figure 10. The magnetopause regions encountered by Polar during 1005–1016 UT on June 19, 1998. The upper panel presents the magnetic field clock angle. The second panel shows the magnetic field magnitude. The third panel presents plasma density from HYDRA (circles) and derived from the spacecraft potential using the relation introduced by *Escoubet et al.* [1997]. The fourth panel presents the energy components in the system: thermal energy density $E_t = nT_i$ is shown by crosses (black line), magnetic energy density $E_{mag} = B^2/2\mu_0$ by circles (blue line) and kinetic energy density $E_k = nm_i v_i^2/2$ by triangles (green line). Total energy $E_{tot} = E_t + E_{mag} + E_k$ is shown by dots (red line). The lower panel shows the components of ion velocities parallel to the magnetopause (GSE Y). The $\mathbf{E} \times \mathbf{B}$ velocity is shown by a solid line, ion velocity perpendicular to $\mathbf{B}$ from HYDRA by crosses and the total ion velocity by circles.

pressure stays approximately constant. Region 4, which is observed during intervals 1008:20–1008:45 UT and 1009:10–1009:50 UT, is detected as a region of plasma flow perpendicular to $\mathbf{B}$ (total velocity is of the order of the $\mathbf{E} \times \mathbf{B}$ velocity) with a strong depression of the magnetic field. The plasma velocity here approaches the local Alfvén velocity, which is locally lower than in the regions 1 and 1′, and which is consistent with Alfvénic propagation of the bulge. Plasma energetics is controlled mainly by the thermal energy and the plasma beta can be very high locally, but generally $\beta_\perp = 2\mu_0 p_\perp / B^2 \geq 1$.

[33] The MP crossing is characterized by the $\sim150°$ rotation in magnetic field and the corresponding density jump from 1 cm^{-3} to 6 cm^{-3} seen at 1008:45 UT. Total magnetic field strength drops as low as 10 nT in the center of the crossing. The MP is followed by Region 2′ (MSBL), identified by the presence of counterstreaming plasma populations (the antiparallel inflowing cold plasma, and the parallel heated/accelerated plasma) and the general decrease in parallel flow velocity, which still has a different direction from the antisunward inflow of about 50 km/s observed in the SH after 1041 UT. The magnetic field on the magnetospheric side of the boundary (80–90 nT) is somewhat stronger than in the MSBL (75–80 nT). Nested minimum variance (MV) analysis reveals that the magnetic field variations are confined to a plane, the normal to which

Polar 1998-06-19   142 data points

Eigenvalues:

3158.35	309.37	23.20

Averages:

Bmax:-3.54   Bint: -3.04   Bmin:10.74

Rotation Matrix:

0.21	0.94	-0.28
0.79	0.00	0.61
0.57	-0.35	-0.74

Figure 11. Hodogram of the magnetic field in LMN coordinates computed using MVA technique for the period 1008:36–1008:53 UT on June 19, 1998. Left and right panels show L-M and L-N representations.

is well determined as indicated by the value 13.4 for the ratio of intermediate-to-minimum eigenvalues. A hodogram of the magnetic field in the MV frame is presented in Figure 11. The average normal magnetic field component i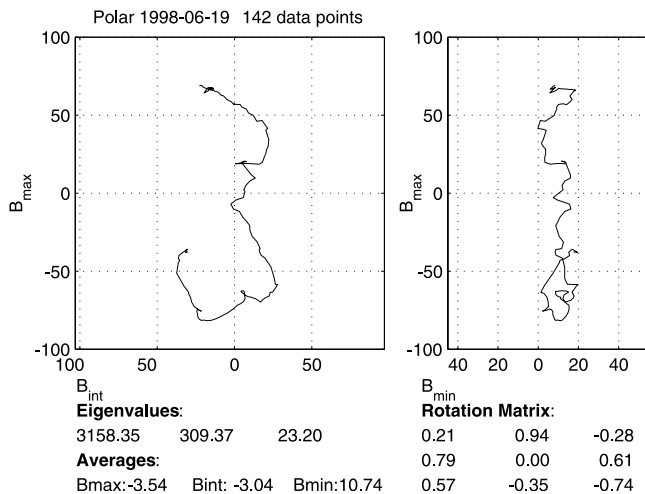s significant ($\sim$10 nT) and the normal, $\mathbf{n} = (0.57, -0.35, -0.74)$ GSE, is approximately perpendicular to the direction of the normal associated with the model MP. Such a discrepancy can be explained by the fact that Polar is located inside the cusp, 2.7 R_E away from the model MP, and the observed normal direction may deviate significantly from the model. A good de Hoffmann-Teller frame was found using electric and magnetic field measurements for the interval shown in Figure 11. Knowing de Hoffmann-Teller velocity V_{dHT}, we can calculate the normal velocity of the MP, $V_n = \mathbf{V}_{dHT} \cdot \mathbf{n}$, which gives $\sim$$-30$ km/s, meaning the MP is moving earthward. This gives the width of the region in which a good MV frame is present, and thus $B_n \neq 0$ (MP thickness), of $\sim$500 km, which is of the order of two proton gyroradii in the MSBL. The evidence for the MP being locally open is good. The Walén test for this interval failed probably due to the fact that the spacecraft crosses the boundary very quickly (narrow boundary) and then immediately returns back (part of the hodogram between points 4 and 5 in Figure 11), leaving us with a very short measurement of the MSBL. Hence there are too few measurement points for plasma moments (resolution is 13.8 sec), and these points are averaged over significant variations. However, Walén tests are satisfied during later, slower MP crossings.

[34] The more complicated backward magnetopause crossing seen at 1009:10 UT in Figure 10 (which includes two large magnetic field rotations) brings Polar back to Region 4 and then to Region 3. Region 3 is rather extended at this time, and plasma density increased in comparison with the first encounter of Region 3. The decaying ion flux parallel to **B** is observed until 1015:35 UT, when it becomes dominated by antiparallel ions (most probably reflected from ionosphere) which define the exit from the bulge.

[35] The later Polar encounters with the energetic ion injection events at 1017, 1027 UT, and later (described in section 2.3) may be explained in a similar way. Generally, Polar moves out from the MS but stays close to the MP. The ion dispersion is less pronounced meaning that the spacecraft came closer to the reconnection point. The bulge is less elongated, and the properties of Region 4 are observed most of the time (see the regions of low-B and perpendicular plasma flow between 1032 and 1040 UT).

[36] Now we discuss the essential differences which help us to distinguish observations of the "bulged MP" produced by transient reconnection discussed above from the observations of MP with ongoing steady reconnection. Our observations are done mainly on the magnetospheric side of the MP, and we will compare two parts of the orbit: (1) the part preceding the crossing of the MP, and (2) the part following the return crossing of the MP. In the case of "bulged MP," bulges move much faster along the MP ($v \sim V_A$) than the normal motion of the MP, and the spacecraft will sense a change in plasma properties along the bulge. Therefore we can expect to observe plasma properties typical for the front part of the bulge before the MP crossing (part 1), and plasma properties typical for the rear part of the bulge after the return MP crossing (part 2). We refer to this case as "asymmetric." In the case of steady reconnection the MP structure is not evolving in time. The observed changes are caused by a change in distance to the MP, and thus part (1) must be similar to part (2) with a reversed time axis. This case is referred to as "symmetric."

[37] If we apply the considerations above to the ion injection events observed at 1006, 1017, and 1027 UT, we clearly see the same pattern for the ion flow in all of these events: ion flows with increasing density and decreasing energy which start in part (1) and continue in part (2) (best seen in the event at 1017 UT). This is consistent with the "asymmetric" pattern described above. In the "symmetric" case, where ion energy depends only on distance to the MP, we should see different signs of energy dispersion (increasing and decreasing) in parts (1) and (2). As a decreasing energy dispersion is the only type of dispersion observed, we conclude that the observed configuration is best explained by the "asymmetric" picture produced by transient reconnection. Additional strong evidence in favor of a transient reconnection mechanism comes from ground observations in the conjugate point as discussed in the next section.

3.2. Ground Observations

[38] Our hypothesis of transient reconnection (FTEs) is supported by ground observations. In this section we show that these ground observations are in good agreement with what is expected for a ground signature of an FTE. The main features observed in the footprint of Polar in association with transient events at the MP are enhancements of convection and electron precipitation.

[39] The direction of the convection change in the ionosphere is governed by motion of the reconnected flux tube. For the case of IMF dominated by B_y the motion of the reconnected flux tube is affected mainly by the magnetic tension ($\mathbf{j} \times \mathbf{B}$) force directed opposite to B_y. During the initial stage this motion is the fastest ($v_y \sim V_A$). After a time

delay defined by the Alfvén wave travel time, the motion at the MP is transferred to the ionosphere. This can be followed in the data as an enhancement of the eastward (as predicted in our case by the sign of B_y) convection channel observed in the ISR and magnetometer data, which is nearly simultaneous with the onset of the ion injection at the MP. In addition to this eastward motion, we observe a noticeable poleward motion caused by the SH flow dragging flux tubes tailward. The duration of reconnection events observed by Polar (∼10 min) is significantly longer than the propagation time of the Alfvén wave (∼1 min), and we observe the response of the ionospheric convection to individual FTEs. Precipitating electrons inside the open flux tube also cause UV auroral emissions. The time resolution for UVI is ∼3 minutes and it is not possible to follow the motion of aurora related to evolution of the FTE – however the switching on and off of the aurora is clearly observed. UVI also gives a good view of the global extent of the FTE signature. Typically, the UV aurora has a width of several degrees in latitude and extends for several hours of MLT. However, the brightest UV spots are rather localized and have a size below 1 hour MLT. Such a significant longitudinal extent of the aurora supports the view that FTEs are not point-like but rather extended, and that reconnection affects a significant area at the MP [*Milan et al.*, 2000].

[40] The poleward motion of enhanced electrojet and convection, seen from about 0945 until 1030 UT, is mainly due to a contraction of the polar cap (area of open flux) occurring after the IMF turning from southward to northward which is seen at 0927 UT by Geotail. During the period of southward IMF open flux was probably added at a high rate to the polar cap as a result of reconnection on the dayside MP. At the same time open flux was removed by reconnection in the magnetotail. If the tail reconnection remained at roughly the same level after the IMF turning, the polar cap would be expected to contract when the dayside reconnection ceases, and reconnection adding open flux at the dawn flank of the MP, which we are investigating here in detail, would be globally less efficient than the dayside merging during the southward IMF. The Polar UVI images do show auroral activity on the nightside throughout the investigated time period which is consistent with a removal of open flux from the polar cap in the tail.

[41] Electrojets inferred from ground magnetometers, and ionospheric plasma convection measured directly and indirectly via ion heating with the ISR, exhibit variations on a time scale of about 10 minutes on top of the large scale poleward motion of enhanced convection. In many previous works similar variations have been associated with reconnection pulses. *Lockwood et al.* [1995] investigated in detail two events seen with the EISCAT radar and a scanning photometer for the 630 nm emission, whether such variations could be due to changes in the Y component of the SH magnetic field with an approximately constant reconnection rate. Following the arguments presented in that study, we conclude that for this event the time variations of the optical emissions at the footprint of the dawn flank seen by Polar indicate a time varying reconnection rate. For a constant reconnection rate one would expect that the optical emissions are always visible although their spatial form might

Figure 12. A schematic of the dayside ionospheric convection, FACs, and the Polar magnetic footprint after 1010 UT on June 19, 1998. Contour lines represent electrostatic equipotentials and colored contours represent FACs (contour interval is 0.1 A/km^2). Blue and red colors represent regions of upward and downward FAC, respectively. Both electrostatic potentials and field aligned currents are calculated using the IZMEM/DMSP model. The magnetic footprint of Polar is marked by the white circle. The electrostatic equipotential contours and FACs are calculated using the IZMEM/DMSP model [*Papitashvili et al.*, 1999] for the IMF B = (6; −11; 3) nT.

vary due to changes of the magnetic field in the magnetosheath. Here, rather, we see bursts of UV emissions from the footprint of the dawn flank. The ion heating and convection shown in Figure 6 indicates that the enhancements do not cease completely in the minima, eg at 10:15 UT. However, the time resolution of the data is not good enough to determine whether they actually go to zero for short periods, and whether the reconnection near the Polar satellite is completely transient.

[42] A schematic of the resulting ionospheric configuration at 1010 UT in terms of convection and field aligned currents (FACs) is presented in Figure 12. The magnetic footprint for the Polar spacecraft (marked by a white circle) is located equatorward of the strong eastward convection channel, which separates the Region 0 and 1 currents. The footprint of the FTE contains the region of strong convection and the aurora seen by UVI (Figure 7), which is likely caused by precipitating magnetosheath electrons with energies less then ∼300 eV (type 2 aurora [*Sandholt et al.*, 1998]). The equatorward part of the FTE overlaps with the Region 1 upward current (cusp), and the poleward part overlaps with the Region 0 downward current or mantle current, which is located poleward from the Polar footprint. The other current region seen in the sector 6–11 MLT is the Region 2 upward current, which bounds the dawn-side convection cell from low latitudes. This contains diffuse aurora caused by the precipitation of high-energy (>∼1 keV) electrons from the dayside exten-

sion of the central plasma sheet (type 3 aurora [*Sandholt et al.*, 1998]), which is seen in Figure 7 and also as an enhancement of E-layer electron density in the ISR measurements (not shown). Such location of the current regions is in agreement with *Watanabe et al.* [1996], but is shifted toward dawn by approximately 3 hours MLT because of the large negative IMF B_y.

[43] Our analysis also implies that the global reconfiguration of the magnetosphere caused by the IMF turning after 0940 UT splits into a sequence of individual FTEs occurring with a period of $\sim$10 min. The flux tubes reconnected earlier are dragged away and new flux tubes are continuously added, and thus impulsively feeding the cusp-mantle current system and the corresponding eastward convection channel, and rearranging the global dayside convection pattern.

4. Summary and Conclusions

[44] We have presented a conjugate observation of transient reconnection events (FTEs) in the northern cusp by the Polar spacecraft and ground instruments in Greenland for an IMF tilted strongly dawnward ($B_y = -11$ nT) and moderately northward ($B_z \sim 3$ nT). Polar location is consistent with being close to the predicted reconnection location for antiparallel merging. The dominant features observed by Polar are impulsive plasma injections in GSE Y direction (consistent with the IMF B_y tension force) and associated crossings of the magnetopause. Magnetic reconnection is the most probable candidate for explaining the observed structure of the plasma flow around the magnetopause. Other mechanisms such as solar wind pressure pulses, Kelvin-Helmholtz and turbulent boundary layer waves can also cause magnetopause motion, but cannot explain accelerated plasma flows and ion energy dispersion.

[45] We find that our observations are best explained by the spacecraft passing bulges of open flux tubes launched intermittently from a reconnection site. We compare the observations to a model of such a bulge, and find good agreement. The boundary separating the magnetosheath boundary layer and the magnetosphere is the only MHD discontinuity present in the bulge, and this boundary can most probably be identified as a rotational discontinuity or intermediate (slow) shock. It contains the largest magnetic field rotation (i.e., magnetopause) and density jump. Two regions are identified inside the bulge: the cusp region, containing plasma flowing parallel to the magnetic field, and the region of plasma flow perpendicular to the magnetic field. The last region is adjacent to the MP and is characterized by strong magnetic field depressions with $\beta \geq 1$, and a flow velocity approaching the local Alfvén velocity. The strongest magnetic field depressions, where $|\mathbf{B}|$ drops to only a few percent of the surrounding value, are found to be related to MP crossings. A similar bulge structure is observed in kinetic simulations of magnetopause reconnection [*Omidi and Winske*, 1995; *Nakamura and Scholer*, 2000]. Inside the bulge, the sheath and magnetospheric plasma populations mix freely along the magnetic field, and thus the plasma and magnetic field parameters change gradually toward their magnetospheric values. The magnetospheric boundary of the bulge is marked by the electron and ion edges and the magnetic barrier exists on the magnetospheric side. As a possible alternative to the transient reconnection mechanism, we have also considered a mechanism where plasma acceleration caused by steady reconnection is combined with some other mechanism causing the magnetopause indentation. We have found that such a mechanism is not able to explain the observed structure of the magnetopause.

[46] The ground response to reconnection events at the MP observed in the magnetic footprint of Polar is also consistent with transient reconnection (FTE). Reconnection bulges are detected at the magnetopause nearly simultaneously with intensification and poleward motion of the cusp electrojet (convection channel). The convection change has a direction consistent with the IMF B_y. A corresponding increase of the auroral intensity is observed at the footprint. The large longitudinal extent ($2-3$ hours MLT) of the ground signature confirms that the reconnection site is rather extended at the MP. The change in the magnetospheric topology caused by the IMF turning from a southward to northward orientation dominated by negative B_y, relaxes in a few $\sim$10 minute long steps as seen from the occurrence of the transient events detected by Polar and the corresponding ionospheric signatures.

[47] We have presented multipoint observations of signatures produced by transient reconnection both in the high-latitude cusp and in the conjugate point on the ground. Complex structure of magnetic field and plasma flow at the magnetopause can be explained in terms of reconnection bulges propagating along the magnetopause. Ionospheric signatures in convection and auroral intensity observed at the footprint are consistent with temporal evolution of the reconnection process at the magnetopause.

References

Dubinin, E., et al. (2002), Polar-Interball coordinated observations of plasma and magnetic field characteristics in the regions of the northern and southern distant cusps, *J. Geophys. Res.*, *107*(A5), 1053, doi:10.1029/2001JA900068.

Escoubet, C. P., A. Pedersen, R. Schmidt, and P. A. Lindqvist (1997), Density in the magnetosphere inferred from ISEE 1 spacecraft potential, *J. Geophys. Res.*, *102*, 17,595.

Fairfield, D. H., W. Baumjohann, G. Paschmann, H. Luhr, and D. G. Sibeck (1990), Upstream pressure variations associated with the bow shock and their effects on the magnetosphere, *J. Geophys. Res.*, *95*, 3773.

Fedorov, A., E. Dubinin, P. Song, A. Skalsky, and E. Budnik (2001), Structure of the flank magnetopause for horizontal IMF: Interball 1 observations, *J. Geophys. Res.*, *106*, 25,419.

Frank, L. A., K. L. Ackerson, W. R. Paterson, J. A. Lee, M. R. English, and G. L. Pickett (1994), The Comprehensive Plasma Instrumentation (CPI) for the Geotail spacecraft, *J. Geomagn. Geoelectr.*, 46, 23–37.

Freeman, M. P., C. J. Farrugia, S. W. H. Cowley, and A. Etemadi (1990), The response of dayside ionospheric convection to the Y-component of the magnetosheath magnetic field: A case study, *Planet. Space Sci.*, 38, 13.

Gosling, J. T., M. F. Thomsen, S. J. Bame, R. C. Elphic, and C. T. Russell (1990), Plasma flow reversals at the dayside magnetopause and the origin of asymmetric polar cap convection, *J. Geophys. Res.*, 95, 8073.

Haerendel, G. (1978), Microscopic plasma processes related to reconnection, *J. Atmos. Terr. Phys.*, 40, 343.

Haerendel, G., and G. Paschmann (1975), Entry of solar wind plasma into the magnetosphere, in *Physics of the Hot Plasma in the Magnetosphere*, edited by B. Hultqvist and L. Stenflo, p. 23, Plenum, New York.

Harvey, P., et al. (1995), The electric field instrument on the POLAR satellite, *Space Sci. Rev.*, 71, 583.

Jorgensen, T. S., E. Friis-Christensen, and J. Wilhjelm (1972), Interplanetary magnetic-field direction and high-latitude ionospheric currents, *J. Geophys. Res.*, 77, 1976.

Kelly, J. D., C. J. Heinselman, J. F. Vickrey, and R. R. Vondrak (1995), The Sondrestrom radar and accompanying ground-based instrumentation, *Space Sci. Rev.*, 71, 797–813.

Kiendl, M. T., V. S. Semenov, I. V. Kubyshkin, H. K. Biernat, R. P. Rijnbeek, and B. P. Besser (1997), MHD analysis of Petschek-type reconnection in non-uniform field and flow geometries, *Space Sci. Rev.*, 79, 709.

Kokubun, S., T. Yamamoto, M. H. Acuna, K. Hayashi, K. Shiokawa, and H. Kawano (1994), The Geotail magnetic field experiment, *J. Geomagn. Geoelectr.*, 46, 7.

La Belle-Hamer, A. L., A. Otto, and L. C. Lee (1995), Magnetic reconnection in the presence of sheared flow and density asymmetry: Applications to the Earth's magnetopause, *J. Geophys. Res.*, 100, 11,875.

Lockwood, M., and C. J. Davis (1996), On the longitudinal extent of magnetopause reconnection pulses, *Ann. Geophys.*, 14, 865.

Lockwood, M., and J. Moen (1996), Ion populations on open field lines within the dayside low-latitude boundary layer: Theory and observations during a transient event, *Geophys. Res. Lett.*, 23, 2895.

Lockwood, M., S. W. H. Cowley, P. E. Sandholt, and U. P. Lovhaug (1995), Causes of plasma flow bursts and dayside auroral transients: An evaluation of two models invoking reconnection pulses and changes in the Y component of the magnetosheath field, *J. Geophys. Res.*, 100, 7613.

Lundin, R., J. Woch, and M. Yamauchi (1991), The present understanding of the cusp, in *Proceedings of the Cusp Workshop*, *Eur. Space Agency Spec. Publ., ESA-SP 330*, 83–95.

Mansurov, S. M. (1969), New evidence of a relationship between magnetic fields in space and on Earth, *Geomagn. Aeron.*, 9, 622.

Maynard, N. C., et al. (2000), Driving dayside convection with northward IMF: Observations by a sounding rocket launched from Svalbard, *J. Geophys. Res.*, 105, 5245.

Milan, S. E., M. Lester, S. W. H. Cowley, and M. Brittnacher (2000), Convection and auroral response to a southward turning of the IMF: Polar UVI, CUTLASS, and IMAGE signatures of transient magnetic flux transfer at the magnetopause, *J. Geophys. Res.*, 105, 15,741.

Moore, T. E., et al. (1995), The Thermal Ion Dynamics Experiment and Plasma Source Instrument, *Space Sci. Rev.*, 71, 409–458.

Mozer, F. S., S. D. Bale, and T. D. Phan (2002), Evidence of diffusion regions at a subsolar magnetopause crossing, *Phys. Rev. Lett.*, 89(1), doi:10.1103/PhysRevLett.89.015002.

Nakamura, M., and M. Scholer (2000), Structure of the magnetopause reconnection layer and of flux transfer events: Ion kinetic effects, *J. Geophys. Res.*, 105, 23,179.

Neudegg, D. A., et al. (2001), The UV aurora and ionospheric flows during flux transfer events, *Ann. Geophys.*, 19, 179.

Omidi, N., and D. Winske (1995), Structure of the magnetopause inferred from one-dimensional hybrid simulations, *J. Geophys. Res.*, 100, 11,935.

Papitashvili, V. O., and F. J. Rich (2002), High-latitude ionospheric convection models derived from Defense Meteorological Satellite Program ion drift observations and parameterized by the interplanetary magnetic field strength and direction, *J. Geophys. Res.*, 107(A8), 1198, doi:10.1029/2001JA000264.

Papitashvili, V. O., B. A. Belov, D. S. Faermark, Y. I. Feldstein, S. A. Golyshev, L. I. Gromova, and A. E. Levitin (1994), Electric potential patterns in the northern and southern polar regions parameterized by the interplanetary magnetic field, *J. Geophys. Res.*, 99, 13,251.

Papitashvili, V. O., F. J. Rich, M. A. Heinemann, and M. R. Hairston (1999), Parameterization of the Defense Meteorological Satellite Program ionospheric electrostatic potentials by the interplanetary magnetic field strength and direction, *J. Geophys. Res.*, 104, 177–184.

Petschek, H. E. (1964), Magnetic field annihilation, *NASA Spec. Publ., NASA-SP 50*, 425–439.

Pinnock, M., A. S. Rodger, J. R. Dudeney, K. B. Baker, R. A. Greenwald, and M. Greenspan (1993), Observations of an enhanced convection channel in the cusp ionosphere, *J. Geophys. Res.*, 98, 3767.

Pinnock, M., G. Chisham, I. J. Coleman, M. P. Freeman, M. Hairston, and J.-P. Villain (2003), The location and rate of dayside reconnection during an interval of southward interplanetary magnetic field, *Ann. Geophys.*, 21, 1467.

Russell, C. T., and R. C. Elphic (1978), Initial ISEE magnetometer results—Magnetopause observations, *Space Sci. Rev.*, 22, 681–715.

Russell, C. T., R. C. Snare, J. D. Means, D. Pierce, D. Dearborn, M. Larson, G. Barr, and G. Le (1995), The GGS/POLAR magnetic fields investigation, *Space Sci. Rev.*, 71, 563.

Sandholt, P. E., M. Lockwood, W. F. Denig, R. C. Elphic, and S. Leontjev (1992), Dynamical auroral structure in the vicinity of the polar cusp: Multipoint observations during southward and northward IMF, *Ann. Geophys.*, 10, 483.

Sandholt, P. E., C. J. Farrugia, J. Moen, O. Noraberg, B. Lybekk, T. Sten, and T. Hansen (1998), A classification of dayside auroral forms and activities as a function of interplanetary magnetic field orientation, *J. Geophys. Res.*, 103, 23,325.

Savin, S., N. L. Borodkova, E. Y. Budnik, A. O. Fedorov, and S. I. Klimov (1998), Interball tail probe measurements in outer cusp and boundary layers, in *Geospace Mass and Energy Flow: Results From the International Solar-Terrestrial Physics Program*, *Geophys. Monogr. Ser.*, vol. 104, edited by D. G. J. L. Horwitz and W. Peterson, pp. 25–44, AGU, Washington, D. C.

Savin, S., et al. (2001), Turbulent boundary layer at the border of geomagnetic trap, *JETP Lett.*, 74, 547.

Savin, S., et al. (2002), Multi-spacecraft tracing of turbulent boundary layer, *Adv. Space Res.*, 30, 2821–2830.

Scholer, M. (1989), Asymmetric time-dependent and stationary magnetic reconnection at the dayside magnetopause, *J. Geophys. Res.*, 94, 15,099.

Scudder, J. D., et al. (1995), HYDRA—A 3-dimensional electron and ion hot plasma instrument for the POLAR spacecraft of the GGS mission, *Space Sci. Rev.*, 71, 459.

Scudder, J. D., F. S. Mozer, N. C. Maynard, and C. T. Russell (2002), Fingerprints of collisionless reconnection at the separator: 1. Ambipolar-Hall signatures, *J. Geophys. Res.*, 107(A10), 1294, doi:10.1029/2001JA000126.

Semenov, V. S., I. V. Kubyshkin, V. V. Lebedeva, M. V. Sidneva, H. K. Biernat, M. F. Heyn, B. P. Besser, and R. P. Rijnbeek (1992), Time-dependent localized reconnection of skewed magnetic fields, *J. Geophys. Res.*, 97, 4251.

Semenov, V. S., I. V. Kubyshkin, M. T. Kiendl, H. K. Biernat, R. P. Rijnbeek, and B. P. Besser (1997), Energetics of reconnection: A reply, *Space Sci. Rev.*, 82, 451.

Shue, J. H., et al. (1998), Magnetopause location under extreme solar wind conditions, *J. Geophys. Res.*, 103, 17,691.

Sibeck, D. G., and P. T. Newell (1995), Pressure-pulse driven surface waves at the magnetopause: A rebuttal, *J. Geophys. Res.*, 100, 21,773.

Sibeck, D. G., et al. (1989), The magnetospheric response to 8-minute period strong-amplitude upstream pressure variations, *J. Geophys. Res.*, 94, 2505.

Sibeck, D. G., N. B. Trivedi, E. Zesta, R. B. Decker, H. J. Singer, A. Szabo, H. Tachihara, and J. Watermann (2003), Pressure-pulse interaction with the magnetosphere and ionosphere, *J. Geophys. Res.*, 108(A2), 1095, doi:10.1029/2002JA009675.

Siscoe, G. L., G. M. Erickson, B. U. O. Sonnerup, N. C. Maynard, K. D. Siebert, D. R. Weimer, and W. W. White (2000), Deflected magnetosheath flow at the high-latitude magnetopause, *J. Geophys. Res.*, 105, 12,851.

Smets, R., D. Delcourt, G. Chanteur, and T. E. Moore (2002), On the incidence of Kelvin-Helmholtz instability for mass exchange process at the Earth's magnetopause, *Ann. Geophys.*, 20, 757–769.

Southwood, D. J., C. J. Farrugia, and M. A. Saunders (1988), What are flux transfer events?, *Planet. Space Sci.*, 36, 503.

Svalgaard, L. (1968), Sector structure of the interplanetary magnetic field and daily variation of the geomagnetic field at high latitudes, p. 11, Danish Meteorol. Inst., Charrlottenlund, Netherlands.

Torr, M. R., et al. (1995), A far ultraviolet imager for the International Solar-Terrestrial Physics mission, *Space Sci. Rev.*, 71, 329.

Tsyganenko, N. A. (2000), Modeling the inner magnetosphere: The asymmetric ring current and region 2 Birkeland currents revisited, *J. Geophys. Res.*, 105, 27,739.

Walthour, D. W., J. T. Gosling, B. U. O. Sonnerup, and C. T. Russell (1994), Observation of anomalous slow-mode shock and reconnection layer in the dayside magnetopause, *J. Geophys. Res.*, 99, 23,705.

Watanabe, M., T. Iijima, and F. J. Rich (1996), Synthesis models of dayside field-aligned currents for strong interplanetary magnetic field By, *J. Geophys. Res.*, *101*, 13,303.

Weimer, D. R. (1996), A flexible, IMF dependent model of high-latitude electric potentials having "space weather" applications, *Geophys. Res. Lett.*, *23*, 2549.

————————————

S. Buchert, Y. Khotyaintsev, K. Stasiewicz, and A. Vaivads, Swedish Institute of Space Physics, Box 537, SE-75121 Uppsala, Sweden. (scb@irfu.se; yuri@irfu.se; ks@irfu.se; andris@irfu.se)

C. J. Farrugia, Space Science Center and Department of Physics, University of New Hampshire, Durham, NH 03824, USA. (charlie.farrugia@unh.edu)

V. O. Papitashvili, Space Physics Research Laboratory, University of Michigan, Ann Arbor, MI 48109, USA. (papita@umich.edu)

B. Popielawska, Space Research Centre, Polish Academy of Sciences, Bartycka 18A, 00-716 Warsaw, Poland. (bpop@cbk.waw.pl)

S. Savin, Space Research Institute (IKI), Profsoyuznaya 84/32, 117997 Moscow, Russia. (ssavin@iki.rssi.ru)

Y.-K. Tung, Space Sciences Laboratory, University of California, Berkeley, CA 94720, USA. (yktung@ssl.berkeley.edu)